Porous, Crystalline, Covalent Organic Frameworks

Adrien P. Côté, *et al.*

Science **310**, 1166 (2005);
DOI: 10.1126/science.1120411

Science (print ISSN 0036-8075; online ISSN 1095-9203) is published weekly, except the last week in December, by the American Association for the Advancement of Science, 1200 New York Avenue NW, Washington, DC 20005.

in the ground state, replacing it with some sort of quantum vortex liquid ground state; or second, that the superflow is being damped by some temperature-dependent mechanism other than vortices (transverse phonons and *umklapp* are two possibilities that are not present in the liquid phase), and this damping only vanishes at zero temperature. Note that here we are always discussing the damping at linear order in the apparent superfluid velocity, thus in linear response to the solid's motion. The actual supersolid transition is where this rate of damping vanishes, so one can have a true superflow in linear response. From these recent experiments at just the one frequency (*2*), we cannot determine where this transition actually happens, or whether it does happen even at zero temperature, although we should conclude from their data that the supersolid transition temperature must be below the dissipation feature, which puts it below 50 mK (*14*). The results of similar experiments at other frequencies should be informative.

References and Notes

1. E. Kim, M. H. W. Chan, *Nature* **427**, 225 (2004).
2. E. Kim, M. H. W. Chan, *Science* **305**, 1941 (2004).
3. A. F. Andreev, I. M. Lifshitz, *JETP* **29**, 1107 (1969).
4. B. A. Fraass, P. R. Granfors, R. O. Simmons, *Phys. Rev. B* **39**, 124 (1989).
5. C. A. Burns, J. M. Goodkind, *J. Low Temp. Phys.* **95**, 695 (1994).
6. W. R. Gardner, J. K. Hoffer, N. E. Phillips, *Phys. Rev. A.* **7**, 1029 (1973).
7. S. M. Heald, D. R. Baer, R. O. Simmons, *Phys. Rev. B* **30**, 2531 (1984).
8. D. S. Greywall, *Phys. Rev. B* **15**, 2604 (1977).
9. P. W. Anderson, *arXiv*, cond-mat/0504731, 7 October 2005.
10. B. Chaudhuri, F. Pederiva, G. V. Chester, *Phys. Rev. B* **60**, 3271 (1999).
11. D. M. Ceperley, B. Bernu, *Phys. Rev. Lett.* **93**, 155303 (2004).
12. D. E. Galli, M. Rossi, L. Reatto, *Phys. Rev. B* **71**, 140506.
13. R. O. Simmons, private communication (2005).
14. In the qualitatively similar oscillator data for superfluid ^{4}He films near their Kosterlitz-Thouless transitions, the actual transition temperature is well below the dissipation feature (*15*).
15. D. J. Bishop, J. D. Reppy, *Phys. Rev. Lett.* **40**, 1727 (1978).

16. We thank M. Chan, R. Simmons, and D. Greywall for helpful discussions. This work was supported in part (D.A.H.) by NSF through grant DMR-0213706.

9 August 2005; accepted 13 October 2005
Published online 3 November 2005;
10.1126/science.1118625
Include this information when citing this paper.

Porous, Crystalline, Covalent Organic Frameworks

Adrien P. Côté,[1]* Annabelle I. Benin,[1] Nathan W. Ockwig,[1] Michael O'Keeffe,[2] Adam J. Matzger,[1] Omar M. Yaghi[1]*

Covalent organic frameworks (COFs) have been designed and successfully synthesized by condensation reactions of phenyl diboronic acid $\{C_6H_4[B(OH)_2]_2\}$ and hexahydroxytriphenylene $[C_{18}H_6(OH)_6]$. Powder x-ray diffraction studies of the highly crystalline products $(C_3H_2BO)_6\bullet(C_9H_{12})_1$ (COF-1) and $C_9H_4BO_2$ (COF-5) revealed expanded porous graphitic layers that are either staggered (COF-1, *P*6$_3$/*mmc*) or eclipsed (COF-5, *P*6/*mmm*). Their crystal structures are entirely held by strong bonds between B, C, and O atoms to form rigid porous architectures with pore sizes ranging from 7 to 27 angstroms. COF-1 and COF-5 exhibit high thermal stability (to temperatures up to 500° to 600°C), permanent porosity, and high surface areas (711 and 1590 square meters per gram, respectively).

The design and synthesis of crystalline extended organic structures in which the building blocks are linked by strong covalent bonds are undeveloped areas of research. It is widely believed that the required microscopic reversibility of the crystallization of linked organic molecules into such solids is difficult if not impossible to achieve (the crystallization problem). The lack of crystalline cross-linked polymers is often cited as evidence in support of this view (*1*). Recently, we embarked on a program aimed at challenging this notion by constructing porous, crystalline, covalent organic frameworks (COFs) solely from light elements (H, B, C, N, and O) that are known to form strong covalent bonds in well-established and useful materials such as diamond, graphite, and boron nitride. The successful realization of COF materials through molecular building blocks would provide covalent frameworks that could be functionalized into lightweight materials optimized for gas storage, photonic, and catalytic applications.

We report a general design strategy and its implementation for the synthesis and crystallization of micro- and mesoporous crystalline COFs. These materials have rigid structures, exceptional thermal stabilities (to temperatures up to 600°C), and low densities, and they exhibit permanent porosity with specific surface areas surpassing those of well-known zeolites and porous silicates. The first two members, COF-1 $[(C_3H_2BO)_6\bullet(C_9H_{12})_1]$ and COF-5 $(C_9H_4BO_2)$, can be synthesized using a simple "one-pot" procedure under mild reaction conditions that are efficient and high-yielding.

To date, attempts to prepare COFs have generally focused on synthesizing porous organic polymers with nonordered structures or densely packed linear polymers that have one-dimensional (1D) crystalline structures (*1*–*6*). An approach involving indirect multistep synthesis of open frameworks templated from molecular solids has also been pursued, but does not give crystalline or fully linked materials (*7*, *8*). Our strategy for synthesizing crystalline COFs involves using one-step condensation reactions of discrete molecules known to produce six- and five-membered rings that can be appropriated for the synthesis of their extended analogs, as shown in Fig. 1.

The synthesis of COF-1 is based on the molecular dehydration reaction (Fig. 1A), in which three boronic acid molecules converge to form a planar six-membered B_3O_3 (boroxine) ring with the elimination of three water molecules. Typically, such molecular structures of cyclotrimerized boronic acids are held in planar conformations by $C–H_{(o\text{-}C_6H_4)}\cdots O_{(BO)}$ [2.975(2) Å] hydrogen bonds (*9*). With this knowledge, we extended this reaction to 1,4-benzenediboronic acid (BDBA), in which a layered hexagonal framework was expected to form upon dehydration as shown in Fig. 1B. For COF-5, we used an analogous condensation reaction. The dehydration reaction between phenylboronic acid and 2,3,6,7,10,11-hexahydroxytriphenylene (HHTP), a trigonal building block, generates a five-membered BO_2C_2 ring (Fig. 1C). From the structural data of this discrete molecular fragment (*10*), an entirely coplanar extended sheet structure was expected to form, according to Fig. 1D.

COF-1 was synthesized by the heating of BDBA at 120°C for 72 hours under a mesitylene-dioxane solution in a sealed Pyrex tube (*11*). These conditions allowed the dehydration of BDBA to proceed slowly. The sparing solubility of BDBA in this solvent system controls the diffusion of the building blocks into solution and facilitates the nucleation of a crystalline material, whereas the use of a closed reaction system sustains the availability of H_2O for maintaining reversible conditions conducive to crystallite growth. After being heated and washed with acetone, COF-1 was isolated as a white powder in 71% yield based on BDBA. With the use of similar reaction conditions, COF-5 was synthesized in 73% yield from a 3:2 stoichiometric ratio of BDBA

[1]Materials Design and Discovery Group, Department of Chemistry, University of Michigan, 930 North University Avenue, Ann Arbor, MI 48109–1055, USA. [2]Department of Chemistry and Biochemistry, Arizona State University, Tempe, AZ 85287–1604, USA.

*To whom correspondence should be addressed. E-mail: oyaghi@umich.edu (O.M.Y.); apcote@umich.edu (A.P.C.)

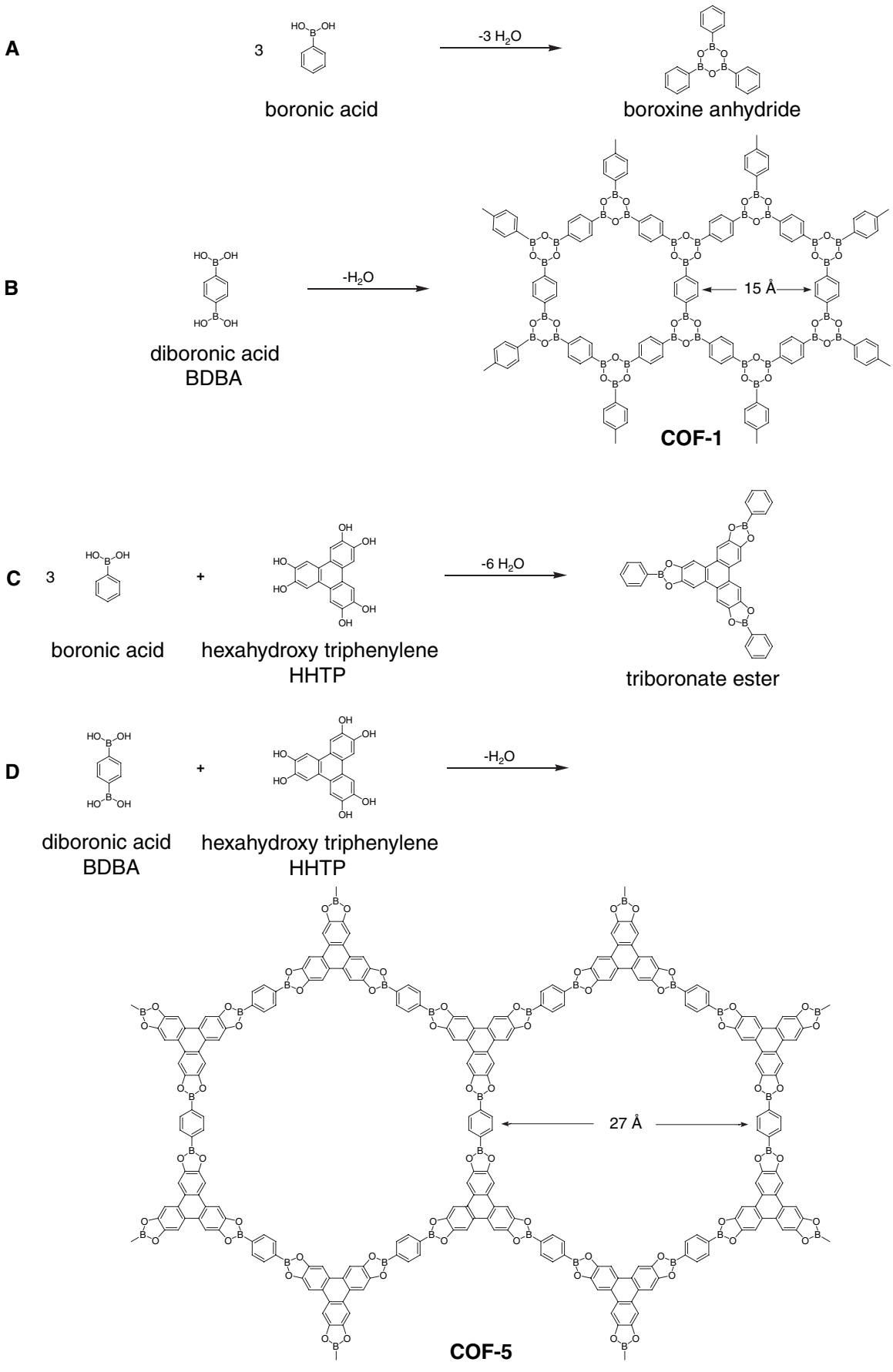

Fig. 1. (**A** to **D**) Condensation reactions of boronic acids used to produce discrete molecules and extended COFs.

to HHTP. After being washed with acetone, COF-5 was obtained as a gray-purple solid, the color of which was due to a small amount of oxidized HHTP formed during the reaction that ultimately occupied the pores of COF-5.

Powder x-ray diffraction (PXRD) analysis of both products confirmed the crystallinity of the COFs and revealed no diffraction peaks that could be attributed to starting materials or their known solvates (Fig. 2, A and E). Furthermore, the phase purity was confirmed by exhaustive scanning electron microscopy (SEM) imaging of the products from multiple reactions where only one morphologically unique crystallite could be found for each COF (Fig. 2, B and F). The Fourier transform infrared (FTIR) spectra of both materials indicated the formation of the expected boron-based ring groups in COF-1 and COF-5, displaying the bands corresponding to the respective boroxine and boronate ester rings; the hydroxyl bands of the starting materials were strongly attenuated in the COF materials (Fig. 2, C and G) (*11*). The ^{11}B solid-state nuclear magnetic resonance (NMR) spectra of the COFs, which do not match that of BDBA, were collected and found to be coincident to those obtained for the molecular model compounds shown in Fig. 1, A and C (Fig. 2, D and H). The line shapes obtained from quadripolar ^{11}B spectra are highly sensitive to the immediate chemical and geometrical bonding environment of boron (*12*). Thus, the nearly identical line shapes of COF-1 and COF-5 as compared to those of their respective boroxine and boronate ester model compounds show that the expected boron-containing rings for these materials had indeed been formed.

In order to confirm that the phases observed from PXRD measurements were indeed those targeted, we modeled the possible extended structures that could be formed from the trigonal boronic molecular units, using the *Cerius*^{2} chemical structure–modeling software suite (*13*). Simulated powder patterns were calculated from these models and compared with the experimentally observed data (Fig. 2, A and E). Given that planar 2D organic sheets were expected to form, layered crystal structures were modeled, in which two distinct stacking possibilities for the organic sheets were considered: (i) a staggered AB arrangement analogous to the packing of graphite sheets, where three-connected vertices (carbon atoms) lie over the center of the six-membered rings of neighboring graphite layers; and (ii) an eclipsed arrangement, in which atoms of adjacent sheets lie directly over each other, as in boron nitride. Like their inorganic counterparts, the staggered and eclipsed models have $P6_3/mmc$ and $P6/mmm$ symmetry, respectively, and each would exhibit distinct diffraction patterns because each space group has a distinct set of symmetry-imposed reflection conditions.

Patterns calculated from the *Cerius*^{2} models also reflect the expected peak intensities, because the x-ray scattering power, positions of framework atoms, and presence of guest molecules are also taken into account. The experimental powder patterns as compared to these calculated models are displayed in Fig. 2, A and E, where there is a close correspondence between the peak positions and intensities for the staggered graphitic model for COF-1 and the eclipsed boron nitride arrangement for COF-5, thus substantiating that these are indeed the targeted layered structures.

Indexing of the experimental x-ray patterns unambiguously gave unit cell parameters nearly equivalent to those determined from the models. To obtain the experimental values, we freely refined the unit cell parameters using full pattern decomposition and profile fitting of the diffraction patterns using a model-biased Le Bail routine [COF-1: calculated: $a = b = 15.6259$, $c = 6.7005$ Å; measured: $a = b = 15.420(1)$, $c = 6.655(4)$ Å. COF-5: calculated: $a = b = 30.0198$, $c = 3.404$ Å; measured: $a = b = 29.70(1)$, $c = 3.460(2)$] (*14*). Peak broadening, asymmetry, and zero-shift errors were accounted for in a calculated diffraction profile and refined against the observed scattering to extract the intensities (F_{obs}) for each structure. The blue difference plots, in Fig. 2, A and E, indicate that the degree of fitting is acceptable for the refined profile (including unit cell parameters).

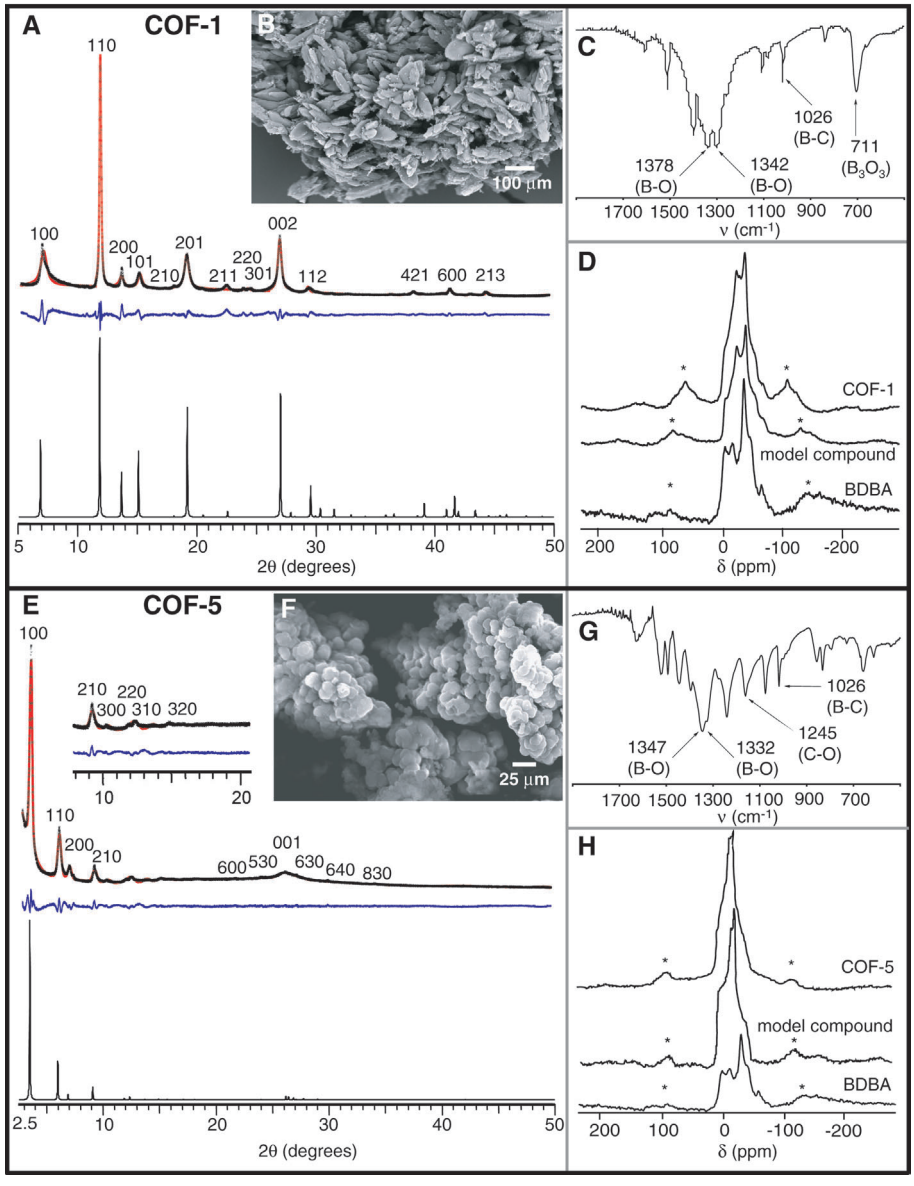

Fig. 2. Physical characterization of COF-1 (**A** to **D**) and COF-5 (**E** to **H**) (*24*). [(A) and (E)] X-ray analysis of (A) COF-1 and (E) COF-5 with the observed pattern in black, the refined profile in red, and the difference plot in blue (observed minus refined profiles). The bottom trace is the calculated PXRD pattern from *Cerius*^{2}. [(B) and (F)] SEM images of bulk COF. [(C) and (G)] FTIR spectra highlighting the characteristic boron functional group bands of (C) COF-1 and (G) COF-5. [(D) and (H)] ^{11}B magic-angle spinning NMR spectra of (top) COF, (middle) model compound, and (bottom) BDBA for (D) COF-1 and (H) COF-5. Asterisks indicate spinning side-band peaks.

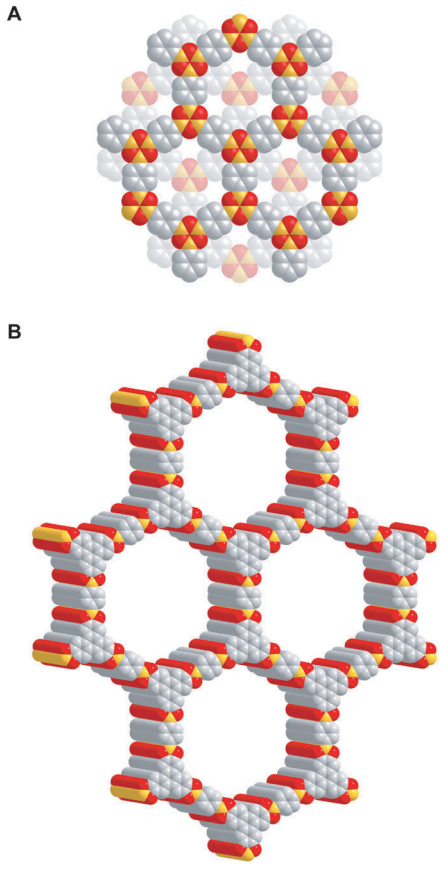

Fig. 3. Structural representations of (**A**) COF-1 and (**B**) COF-5 based on powder diffraction and modeling projected along their *c* axes (H atoms are omitted). Carbon, boron, and oxygen are represented as gray, orange, and red spheres, respectively.

The number of observed peaks for COF-1 and COF-5 were too few to permit refinement of atom positions in the models using Rietveld methods. Nevertheless, the initial intensities calculated from the *Cerius*[2] structures used in the extraction represent viable models for these data, because statistically reasonable profiles could be obtained from readily convergent refinements [COF-1: wR_p = 0.1122, R_p = 0.0871, χ^2 = 10.43 (where R_p and wR_p are profile-fitting factors); COF-5: wR_p = 0.0635, R_p = 0.0476, χ^2 = 18.46] (*15*).

The structure of COF-1 can be derived from graphite by replacing each C atom with a B_3O_3 boroxine unit and each C–C bond by a ditopic phenylene unit (Fig. 3A). As expected, the interlayer spacing of COF-1 is near that of graphite [3.328(4) versus 3.348(1) Å] (*16*). Given the presence of 15.1 Å perforations within the layers of COF-1 arising from expansion, a 1D pore exists throughout the material with an aperture of 7.0 Å defined by the van der Waals distance between phenyl and B_3O_3 rings of adjacent layers (Fig. 3A). Using ^{13}C solid-state NMR spectroscopy, we found that the pores were occupied by mesitylene guest molecules incorporated during the reaction (*11*).

To determine the thermal stability of COF-1 in the absence of guests, a thermogravimetric analysis was done on the as-synthesized materials. Mesitylene guests can be removed by heating the material to 200°C, with an accompanying mass loss of 21%; this decrease corroborates the formula determined from elemental microanalysis as $(C_3H_2BO)_6\bullet(C_9H_{12})_1$, which corresponds to one guest per cavity. There is no indication from spectroscopic analysis that degradation of the covalently bonded layers results from guest removal (*11*, *15*). COF-1 remains crystalline after evacuation of mesitylene, with some shifting of the layers being evident (fig. S21).

The structure of COF-5 can be derived from that of graphite, except that the layers stack in an eclipsed fashion as observed in boron nitride (Fig. 3B) to form a hexagonal array of 1D mesopores whose diameter is 27 Å. A notable disorder in the spacing of the layers is evident from the broad (001) peak in the powder pattern. An interlayer spacing of 3.460(2) Å (interlayer spacing = d_{001}) can be calculated and is comparable to the 3.33(1) Å spacing of boron nitride (*17*). Within examples of ordered mesoporous channel structures, periodicity at the 3 Å level has only been achieved on one occasion, in a surfactant-templated organosilicate (*18*).

We attribute the formation of an eclipsed structure over a staggered structure in this case to the presence of the HHTP unit that bestows a larger number of overriding π-π interactions to guide layer stacking rather than by B···O interactions alone. Unlike COF-1, the included guests (HHTP starting material) in COF-5 are nonvolatile. Thus, they were exchanged by soaking the as-synthesized crystals in acetone for 12 hours. The color of COF-5 changes to light gray because the highly colored oxidized form of HHTP comprises a fraction of the guests as determined from the mass spectrum of the acetone supernatant after exchange (*11*). As with COF-1, upon removal of guests, no degradation of COF-5 was evident from spectroscopic analysis, and x-ray analysis revealed that the stacking of the layers was preserved (*11*). A reliable formulation of the evacuated form of COF-5 was found by elemental microanalysis to be $C_9H_4BO_3$, corresponding to the expected formula.

The architectural stability and porosity of COF-1 and COF-5 were confirmed by measuring the N_2 gas adsorption of the guest-free material. A sample of as-synthesized COF-1 was evacuated with a dynamic 10^{-5} Torr vacuum pressure and heated to 150°C for 12 hours to remove all the guests. This sample was used for measurement of the isotherm at 77 K from 0 to 1 bar (1 bar = P_o), which showed a very sharp uptake at P/P_o from 10^{-5} to 10^{-1}, a signature feature of a microporous material (Fig. 4A). The Brunauer-Emmett-Teller (BET) model was applied to the isotherm for P/P_o between 0.04 and 0.1, which resulted in an apparent surface area of S_{BET} = 711 $m^2\ g^{-1}$; the pore volume V_p = 0.32 $cm^3\ g^{-1}$ at P/P_o = 0.90. These values surpass those of other layered materials, including graphite (10 $m^2\ g^{-1}$), clays (10 to 100 $m^2\ g^{-1}$), and pillared clays (50 to 300 $m^2\ g^{-1}$) and are in the range of the most porous zeolites and many porous carbons (*19*). At higher pressures, a slow rise in the isotherm occurs because of the existence of a small population of external mesopores between the crystallites; this feature is not uncommon for particles with platelet morphologies (*19*). The total surface area was calculated to be 711 $m^2\ g^{-1}$, with a micropore contribution of 587 $m^2\ g^{-1}$ (83%) and mesopore contribution of 124 $m^2\ g^{-1}$ (17%) from de Boer statistical thickness (*t*-plot) analysis (*19*).

We collected Ar and high-temperature CO_2 isotherms in the same pressure range, which we fit with density functional theory (DFT) models that account for the microscopic behavior of sorbed molecules (*11*, *20*). From these calculations, a very reliable pore size distribution can be calculated and is shown Fig. 4C. Corroborating the results from *t*-plot analysis, the distribution is largely populated between 6 and 12 Å and matches the micropore dimensions expected from the structure of COF-1; the range from 28 to 45 Å arises from the aforementioned interparticle mesopores. The cumulative pore volume (0.34 $cm^3\ g^{-1}$) and surface area (640 $m^2\ g^{-1}$) from DFT calculations compare favorably with the values determined above. The isotherm for COF-1 is fully reversible and reproducible: a feature of stable materials whose structures exhibit permanent porosity.

The N_2 adsorption isotherm of COF-5, measured under the same conditions as COF-1, shows a reversible type-IV isotherm characteristic of mesoporous materials (Fig. 4B). There are two notable features in this isotherm. The first is a sharp step observed for pore condensation for P/P_o from 0.11 to 0.15, caused by a narrow distribution of mesopores (*21*); this finding was supported by DFT calculations with a pore width of 27 Å dominating the distribution (Fig. 4D) (*22*). Second, the absence of hysteresis during desorption is a common feature of materials containing hexagonally aligned 1D mesopores with widths <40 Å (*21*). It is also apparent from the pore size distribution that 23% of the total surface area can be assigned to micropore uptake. Because an impurity phase has not been encountered, we speculate that the origin of the significant low-pressure uptake arises from partially slipped organic sheets that create grottos along the mesopore walls where adsorbate molecules are more strongly bound. The BET surface area of COF-5 was 1590 $m^2\ g^{-1}$, which corresponds to a mesopore volume of 0.998 $cm^3\ g^{-1}$, values that are greater than double that reported for 26 Å Mobile Crystalline Material 41 (MCM-41) (680 $m^2\ g^{-1}$

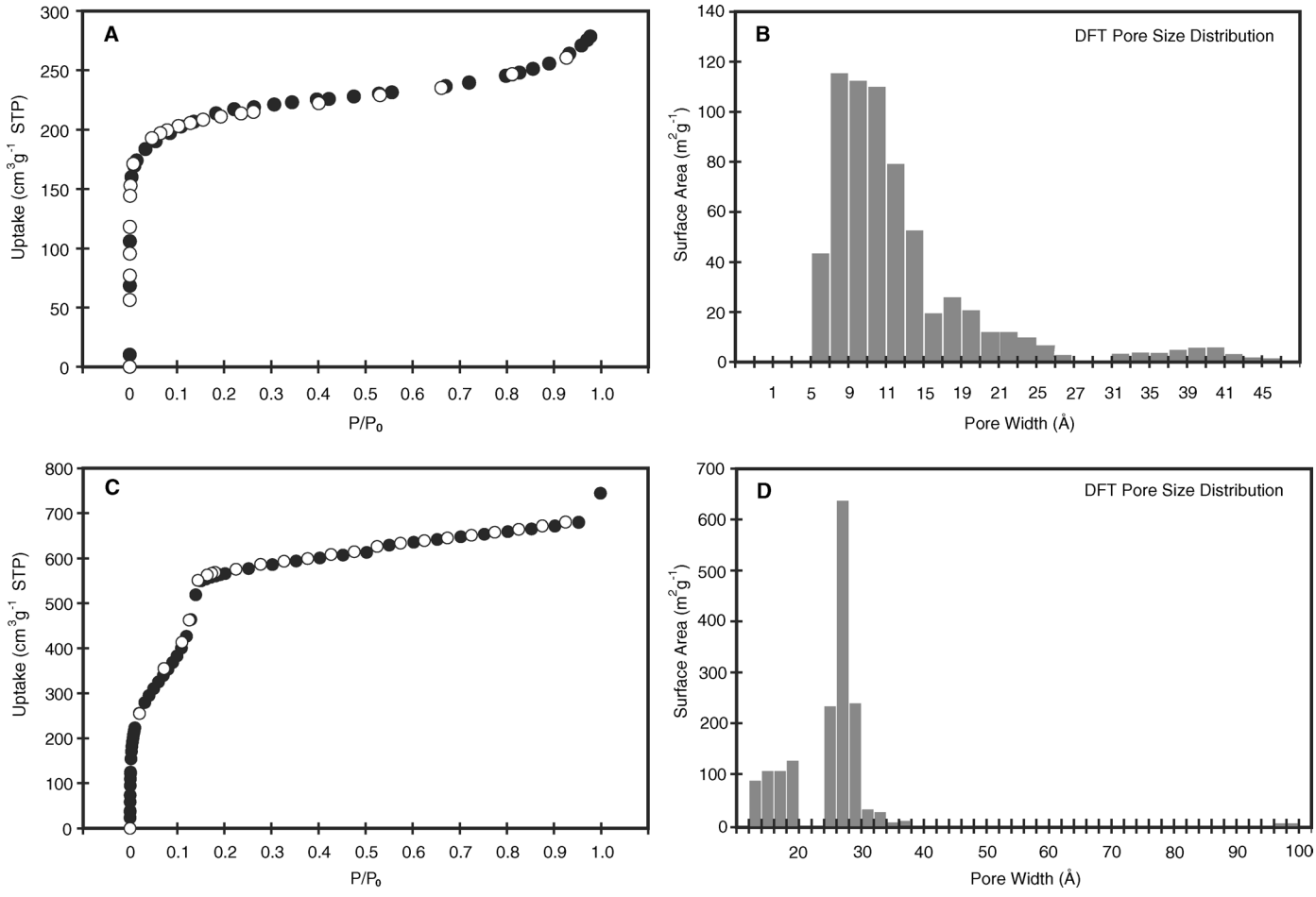

Fig. 4. Nitrogen gas adsorption isotherms for COF-1 (**A**) and COF-5 (**C**) measured at 77 K and pore size histograms for (**B**) COF-1 and (**D**) COF-5 calculated after fitting DFT models to adsorption data.

and 0.26 cm^3 g^{-1}) (*23*) and exceed that of the highest reported surface area of 1300 m^2 g^{-1} for a macroporous ordered silica (*21*).

References and Notes

1. P. J. Florey, *Principles of Polymer Chemistry* (Cornell Univ. Press, Ithaca, NY, 1953).
2. D. T. Vodak *et al.*, *J. Am. Chem. Soc.* **124**, 4942 (2002).
3. H. B. Sonmez, F. Wudl, *Macromolecules* **38**, 1623 (2005).
4. S. M. Curtis *et al.*, *Supramol. Chem.* **17**, 31 (2005).
5. T. Hoang, L. W. Lauher, F. W. Fowler, *J. Am. Chem. Soc.* **124**, 10656 (2002).
6. W. Niu, C. O'Sullivan, B. M. Rambo, M. D. Smith, J. J. Lavigne, *Chem. Commun.* **2005**, 4342 (2005).
7. Z. Xu *et al.*, *Adv. Mater.* **12**, 637 (2001).
8. P. Brunet, E. Demers, T. Maris, G. D. Enright, J. D. Wuest, *Angew. Chem. Int. Ed. Engl.* **42**, 5303 (2003).
9. C. P. Brock, R. P. Minton, K. Niedenzu, *Acta Crystallogr.* **C43**, 1775 (1987).
10. V. F. Zettler, H. D. Hausen, H. D. Hess, *Acta Crystallogr.* **B30**, 1876 (1974).
11. Materials and methods are available as supporting material on *Science* Online. The synthesis of COF-1 was carried out as follows: A Pyrex tube with an outside diameter of 10 mm and an inside diameter of 8 mm was charged with BDBA (25 mg, 0.15 mmol, Aldrich) and 1 ml of a 1:1 v:v solution of mesitylene: dioxane. The tube was flash-frozen at 77 K (in a liquid N_2 bath) and evacuated to an internal pressure of 150 mTorr and flame-sealed. Upon sealing, the length of the tube was reduced to 18 cm. The reaction mixture was heated at 120°C for 72 hours, yielding a white solid at bottom of the tube, which was isolated by filtration and washed with acetone (30 ml). The yield was 17 mg, 71% for $(C_3H_2BO)_6\bullet(C_9H_{12})_1$. The synthesis of COF-5 was carried out as follows: Using the same reaction design as for COF-1, BDBA (12.5 mg, 0.075 mmol, Aldrich) and HHTP (16 mg, 0.050 mmol, TCI) were heated at 100°C for 72 hours to yield a free-flowing, gray-purple powder. The yield was 15 mg, 73% for $C_9H_4BO_2$ after guest removal. No evidence for the self-condensation of BDBA to form COF-1 was observed from the synthesis of COF-5. The reaction of BDBA alone at 100°C was slow, and after 168 hours of heating, produced COF-1 in only 25% yield.
12. C. Gervais, F. Babonneau, *J. Organomet. Chem.* **657**, 75 (2002).
13. *Cerius*^{2} Modeling Environment (Molecular Simulations, San Diego, CA, 1999).
14. A. C. Larson, R. B. VonDreele, *General Structure Analysis System* (*GSAS*) (Los Alamos National Laboratory Report LAUR 86-748, Los Alamos, NM, 2004).
15. Disorder existing in these compounds arises from the stacking of the sheets, as evidenced from the line broadening in the x-ray patterns (turbostratic disorder) and is frequently observed in layered materials. The tailing to a high angle of the (100) lines points to translational faults in the *xy* basal planes of the structures, whereas the broadening of lines corresponding to layer stacking along the *c* axes [(002) for COF-1 and (001) for COF-5] indicates variances in the interlayer spacings, which is more pronounced in COF-5. The construction of the open layers in COF-1 and COF-5 has been established by spectroscopy, and analysis of their gas adsorption isotherms reveals the respective permanent micro- and mesoporosity and pore sizes near those determined from x-ray data. Despite their lack of perfect crystallinity, the investigation and use of COFs as porous materials are not precluded.
16. R. C. Tatar, S. Rabii, *Phys. Rev. B* **13**, **4126** (1982).
17. E. K. Sichel, R. E. Miller, M. S. Abrahams, C. J. Buiocchi, *Phys. Rev. B* **13**, 4607 (1976).
18. S. Inagaki, S. Guan, T. Ohsuna, O. Terasaki, *Nature* **416**, 304 (2002).
19. F. Rouquerol, J. Rouquerol, K. Sing, *Adsorption by Powders and Porous Solids* (Academic Press, London, 2002).
20. R. I. Ravikovitch, A. Vishnyakov, R. Russo, A. V. Neimark, *Langmuir* **16**, 2311 (2000).
21. M. Thommes, in *Nanoporous Materials Science and Engineering*, G. Q. Lu, X. S. Zhao, Eds. (Imperial College Press, London, 2004), chap. 11.
22. M. Kruk, M. Jaroniec, *Chem. Mater.* **12**, 222 (2000).
23. M. Kruk, M. Jaroniec, A. Sayari, *J. Phys. Chem. B* **101**, 583 (1997).
24. Atomic coordinates have been deposited in the Cambridge Crystallographic Database under deposition numbers 287138 (COF-1) and 287139 (COF-5).

25. Supported by NSF, the U.S. Department of Energy, and the Natural Sciences and Engineering Research Council of Canada (a postdoctoral fellowship to A.P.C.). We thank M. V. Wilson and L. W. Beck (University of Michigan) for their valuable assistance with NMR measurements and K. Leinenweber (Arizona State University) for his expert advice regarding x-ray analysis.

Supporting Online Material

www.sciencemag.org/cgi/content/full/310/5751/1166/DC1
Materials and Methods
Figs. S1 to S37
Tables S1 to S4

21 September 2005; accepted 21 October 2005
10.1126/science.1120411